Final Draft of:

Piperlongumine (piplartine) and analogues: Antiproliferative microtubule-destabilising agents

Meegan, M.J., Nathwani, S., Twamley, B., Zisterer, D.M., O'Boyle, N.M.*

European Journal of Medicinal Chemistry

Volume 125, 5 January 2017, Pages 453-463

DOI: http://dx.doi.org/10.1016/j.ejmech.2016.09.048

Piperlongumine (Piplartine) and Analogues: Antiproliferative Microtubule-Destabilising Agents

Mary J. Meegan,[1] Seema Nathwani,[2] Brendan Twamley,[3] Daniela M. Zisterer,[2] Niamh M. O'Boyle[1,2]*

[1]School of Pharmacy and Pharmaceutical Sciences, Trinity College Dublin, Dublin 2, Ireland.

[2]School of Biochemistry & Immunology, Trinity Biomedical Sciences Institute, 152-160 Pearse Street, Trinity College Dublin, Dublin 2, Ireland.

[3]School of Chemistry, Trinity College Dublin, Dublin 2, Ireland.

*Corresponding author; email oboyleni@tcd.ie

ABSTRACT

Piperlongumine (piplartine, **1**) is a small molecule alkaloid that is receiving intense interest due to its antiproliferative and anticancer activities. We investigated the effects of **1** on tubulin and microtubules. Using both an isolated tubulin assay, and a combination of sedimentation and Western blotting, we demonstrated that **1** is a tubulin-destabilising agent. This result was confirmed by immunofluorescence and confocal microscopy, which showed that microtubules in MCF-7 breast cancer cells were depolymerised when treated with **1**. We synthesised a number of analogues of **1** to explore structure-activity relationships. Compound **13** had the best cytotoxic profile of this series, showing potent effects in human breast carcinoma MCF-7 cells whilst being relatively non-toxic to non-tumorigenic MCF-10a cells. These compounds will be further developed as potential clinical candidates for the treatment of breast cancer.

KEYWORDS

Antiproliferative; anticancer; combretastatin A-4; microtubule-destabilizing; piperlongumine; tubulin

1. INTRODUCTION

Cancer is the uncontrolled growth and spread of cells. Annually, 8.2 million deaths are attributable to cancer, an estimated 13% of all deaths worldwide, and breast cancer accounts for over half a million of these. The total number of new cases is expected to rise by 70% over the next two decades [1]. The continuous development of new, cost-effective drug therapies is crucial to increase the range of options available to patients, and to improve their long-term prognosis.

Piperlongumine (also known as piplartine, **1**, Figure 1) is an alkaloid isolated from a number of *Piper* plant species, including the long pepper plant *Piper longum* L. It has a large number of reported uses in traditional medicine, and has demonstrated cytotoxic and antitumour activity [2]. In particular, it was found to be selectively toxic to cancer cells by increasing the level of reactive oxygen species (ROS) and inducing apoptotic cell death, although the exact mechanisms of action remain unclear [3]. Compound **1** has been recently reported to be a direct STAT3 inhibitor [4], a proteasome inhibitor [5], to promote autophagy [6], and to modulate NF-κB and NF-κB-regulated gene products [7].

Compound **1** is a chalcone-type molecule, consisting of two ring systems linked by a α-β-unsaturated carbonyl chain. One of the rings is aromatic and substituted with three methoxy groups, while the second is a piperidinone-type ring containing a conjugated alkene. Compound **1** is structurally similar to a number of known tubulin-targeting antiproliferative compounds. These include combretastatin A-4 (**2**) and chalcone **3** (Figure 1), both containing a trimethoxyphenyl

moiety [8]. An analogue of **2** with a substituted pyridone ring (**4**, Figure 1) also displays potent antitubulin activity [9]. A hybrid of compounds **1** and **2** was recently reported as a tubulin depolymerising agent [10]. Considering these results, we undertook to investigate if **1** has inherent tubulin- and microtubule-targeting activity in breast cancer cells. We also synthesised a number of analogues of **1** to investigate structure-activity relationships of the trimethoxyphenyl group of **1** on the antiproliferative potency in breast cancer cells.

2. RESULTS and DISCUSSION

2.1. Chemistry

Previous research has examined the structure-activity relationships of the piperidinone ring of **1** [11]. Hence, we sought to examine the effects of modifying the trimethoxyphenyl ring. The trimethoxyphenyl ring has repeatedly been shown to be crucial for the tubulin-depolymerising ability of a number of compounds, including colchicine, podophyllotoxin and **2** [12-14]. These trimethoxyphenyl-containing compounds bind at the colchicine-binding site on tubulin, mainly located in the β-subunit. A number of analogues of **1** with different substituents were chosen for synthesis, in order to better understand the contribution of the trimethoxyphenyl ring to the antiproliferative activity of **1**. Synthesis was achieved in two steps *via* the key intermediate 5,6-dihydropyridin-2(1H)-one.

5,6-Dihydropyridin-2(1*H*)-one (**6**) was synthesised in two steps from but-3-en-1-amine *via* N-(but-3-en-1-yl)acrylamide (**5**) (Scheme 1, steps *i* and *ii*). Compound **1** and seven analogues (**7**-**13**) were obtained in moderate yields via a one-pot reaction between **6** and appropriately substituted cinnamic acids, pre-activated with pivaloyl chloride (Scheme 1, steps *iii* and *iv*, 61-72% yield)[15]. ^{1}H NMR coupling constants (15-16 Hz) indicated a *trans* configuration around the linear α,β-

unsaturated double bond. An X-ray crystallographic study of **12** confirmed the structure, featuring a non-planar piperidinone ring and a 3,4-dimethoxyaryl ring (Figure 2). The length of the double bond in the lactam ring agrees with the published structure for **1** (1.329 Å compared to 1.322 Å) [16]. The C-N bonds in the lactam ring are unequal with lengths of 1.482 Å (C1-N6) compared to 1.390 Å (C5-N6). The 3-methoxy and 4-methoxy groups are approximately co-planar with the aromatic ring (torsion angles 5.6 (2)° and 176.8 (13)° respectively). The linear α,β-unsaturated double bond adopts the predicted *trans* configuration, with a bond length of 1.335 Å (1.329 Å reported)[16].

2.2. Biochemistry

2.2.1. Cell Viability

Compound **1** was first tested for its effects on viability in two human cell lines, MCF-7 breast cancer cells and Jurkat T-lymphocytes. The concentration of **1** required to inhibit the growth of MCF-7 and Jurkat cells by 50% (IC_{50}) was determined to be 1.2 ± 0.6 μM and 1.4 ± 0.3 μM respectively at 48 hr (Figure 3A). These are similar to previously reported values for **1** (8 μM in MCF-7 cells and 5 μM in Jurkat cells) [17, 18]. Cell viability results for **1** in a large number of cancer cell lines have been determined and, in general, IC_{50} values range between 1-10 μM [2].

IC_{50} values for compounds **7-13** were found to be between 3.4 and 9.6 μM in MCF-7 cancer cells, with **7**, **12** and **13** showing the best activity (IC_{50} values of 3.5, 3.7 and 3.4 μM respectively)(Table 1). Mono-methoxylated compounds **8**, **9** and **10** showed decreased potency indicating that one methoxy group is detrimental to antiproliferative activity, regardless of its position on the ring (2-, 3-, or 4-methoxy). Comparison of di-methoxylated compounds **11** and **12** reveals that a 2,3-methoxy substitution pattern is preferable to 1,3-methoxy (IC_{50} values of 8.5 and 3.7 μM

respectively). These analogues were also assessed for toxicity using non-tumorigenic MCF-10a mammary epithelial cell line (Figure 3B and Figure S1, Supporting Information). None of the compounds had any effect on viability of MCF-10a cells at a concentration of 1 μM (24 and 48 hr) and minimal effects were noted at 5 μM (>90% viability for all compounds at 24 hr, and >80% viability at 48 hr). The best selectivity at 5 μM was observed for compounds **7**, **12** and **13** (differences of 53, 46 and 48% in cell viability of MCF-10a compared to MCF-7, respectively). Significant effects on MCF-10a cell viability were observed at 10 μM, equal to the effect on MCF-7 viability in most cases. Treatment with **1** (10 μM) caused a 90% reduction in cell viability. This indicates poor selectivity for cancer cells at this concentration, with the exception of compound **13**. Compound **7** showed the highest toxicity at 48 hr (Figure 3B). On the basis of combined results in MCF-7 and MCF-10a cells, compounds **12** and **13** were identified as the best candidates for future development.

2.2.2. Effect of Pre-treatment with Antioxidants on Cellular Viability

Compound **1** has been reported as an agent that increases the level of ROS in cells [3]. To investigate the potential effects of our analogues **7-13** on ROS levels in MCF-7 breast cancer cells, we employed a viability assay in which cells are pre-incubated with an antioxidant prior to treatment with the compound of interest (Figure 4). This assay indicates potential involvement of ROS in a compound's mechanism of action. Two antioxidants were used: N-acetyl cysteine (NAC) and the vitamin E derivative Trolox (6-hydroxy-2,5,7,8-tetramethylchroman-2-carboxylic acid). The antioxidant concentrations used were shown to have no effect on cell viability. Trolox (100 μM and 300 μM) has been shown to be an effective antioxidant in MDA-MB-231 breast cancer cells and MIA PaCa-2 pancreatic cancer cells [19]. We also evaluated a number of known tubulin-destabilising agents [colchicine, **2** and four chalcones (**14-17**, Figure 5)]. These compounds were

chosen on the basis of structural similarity to **1** (all with the exception of colchicine contain a linear double bond linking two ring systems, one of which is substituted with 2 or more methoxy groups), antiproliferative potency, and tubulin-targeting activity. These chalcones were synthesised and characterised by published procedures (compound **14** [8], **15** [20], **16** [8], **17** [21]).

Firstly, the effects of **1** and representative compounds **7**, **12** and **13**, alone and in combination with NAC and Trolox were assessed. Pre-treatment for 1 hr with NAC has a dramatic protective effect on MCF-7 cells at all concentrations of all compounds tested (Figure 4). Viability increases were generally greater than 50%, with the highest increase of 73% (compound **7**, 10 μM). No significant increases in cell viability were noted when cells were pre-treated with Trolox. Similar results show that pre-treatment with NAC but not Trolox has an effect on activity of **1** [19]. Compound **1** is a relatively reactive compound, due to the reactive α,β-unsaturated carbonyl system contained in the piperidinone ring. It has been shown to directly bind to NAC (200 equiv. in Hepes buffer; 24 hr reaction)[19] and to the small-molecule thiol methyl thioglycolate (3 equiv. in DMSO; 72 hr reaction)[11]. It is possible that this reaction occurs in the aqueous media of cell viability assay, thus inactivating the α,β-unsaturated carbonyl group of **1**. This reaction is not possible with Trolox. The same considerations apply to analogues **7**, **12** and **13**. This is a potential reason for the different effects observed with the two different antioxidants. The differing concentrations of NAC and Trolox may also play a part.

Secondly, effects of antioxidant pre-treatment on cell viability were assessed for known tubulin-targeting compounds. Cells pre-treated with NAC showed increased viability for all compounds compared to cells that were not pre-treated (Figure 6). Highest increases were noted for **2** (100 nM; 22%) and chalcone **14** (35%). Increases in viability were greater than 10% for all concentrations of the six compounds evaluated. Similar results were obtained for a lower

concentration of **16** and **17** (1 μM; data not shown). Cells pre-treated with Trolox showed slightly increased viability but effects were generally minimal (Figure 6). The highest increase in viability was 11.4% for **2** (10 μM). Viability was increased by less than 10% for chalcones **14**-**17**.

The results from the viability assay of colchicine, **2** and chalcones **14**-**17** indicate potential ROS involvement in cancer cell death. This has not been reported for **2** or chalcones **14**-**17** previously and is worthy of further investigation. A number of known tubulin-targeting agents also have effects on reactive oxygen species in cells. Paclitaxel, a microtubule-stabilising agent, has been reported to generate ROS by activating plasma-membrane associated NADPH oxidase (NOX)[22]. Vinca alkaloids, clinically used microtubule-destabilising agents, induce apoptosis in lung adenocarcinoma cells via ROS accumulation [23]. Isothiocyanates known to induce oxidative stress have subsequently been shown to induce degradation of cellular tubulin by proteasomes [24]. An analogue of colchicine, Green-1, was reported as increasing ROS production in pancreatic cancer cells and leukaemia cells but its structural modification led to loss of its ability to depolymerise tubulin [25]. It appears that there is a link between ROS levels and the behaviour of microtubules in cells. Given the advanced status of **2** in phase II clinical trials, it is important to fully elucidate its cellular effects [21].

2.2.3. Effects of Piperlongumine on the Cell Cycle and Apoptosis

Further biochemical work was carried out to explore the type of cell death induced by **1**. The effects of **1** on the cell cycle of MCF-7 cells were evaluated. Flow cytometric analysis of propidium iodide stained cells demonstrated simultaneous decreases in the G_0G_1 cell population [16 % and 15 % (24 hr), and 21 % and 19 % (48 hr) for 10 and 20 μM respectively] and increases in the G_2/M cell population [13 %, 16 % and 12 % (24 hr), and 6 %, 15 % and 10 % (48 hr) for 5, 10 and 20

μM respectively] (Figure 7A). There was a small, statistically significant increase in the percentage of apoptotic cells (sub-G_0G_1) after 48 hr (10 and 20 μM of **1**; 4.3 and 4.9% respectively).

Due to the increase in apoptotic cells, further effects of **1** on anti-apoptotic proteins of the Bcl-2 protein family were investigated, namely Bcl-2 and Mcl-1. These proteins contribute to an increased apoptotic threshold in cancer cells and allow cells to survive in stressful environments. Treatment with **1** (10 μM) caused downregulation of the expression of Bcl-2 and Mcl-1 as demonstrated by western blotting (Figure 7B). Expression of Bcl-2 was downregulated at 48 hr, whereas expression of Mcl-1 was evidenced after 72 hr. These results are in agreement with previous reports of **1**-induced apoptosis in MCF-7 cells after 36 hr, evidenced by annexin V/PI double-staining and PARP cleavage [26]. Compound **1** also reportedly induces both apoptosis and necrosis in leukaemia cell lines [17], and apoptosis in Burkitt lymphoma cell lines [27], prostate cancer cells [28], and triple-negative breast cancer cells [18].

Tubulin-destabilising agents often cause increased cell accumulation in the G_2/M phase, due to defective mitotic checkpoints, as found for **1** in MCF-7 cells above. A number of previous studies have noted G_2/M arrest upon treatment with **1**, including in Chinese hamster lung fibroblasts (V79),[29] OVCAR3 human ovarian cancer cells [30] and PC-3 prostate carcinoma cells [28]. This suggests that **1** may potentially target tubulin. The structural similarity of **1** to a number of known tubulin-destabilizing agents (Figure 1) strengthens this hypothesis. To investigate further, specific tubulin assays were performed.

2.2.4. Effects of Piperlongumine on Tubulin Polymerisation and Interaction with Colchicine-Binding Site

The tubulin-targeting properties of **1** were firstly examined in vitro using isolated bovine tubulin (Figure 8A). The effect of test compounds **1** and **7** on tubulin polymerization was determined by reading absorbance at 340 nm over 60 min, as the extent of light-scattering by microtubules is proportional to their degree of polymerisation [31]. Paclitaxel, a known microtubule-stabilising agent, was used as a control and increased the final polymer mass (Figure 8A). Depolymerisation of tubulin and reduction in the final polymer mass was noted for the higher concentration of **1** (25 μM, Figure 8A). A similar but less pronounced effect was seen for compound **7** (25 μM). Compound **1** was selected for further investigation in MCF-7 breast cancer cells and Jurkat T-lymphocytes.

A cellular assay based on sedimentation followed by western blotting were used to examine the effects of **1** on tubulin polymerisation in both MCF-7 and Jurkat cells (Figure 8B). Polymerized and depolymerized microtubules have different solubilities and localize preferentially in the pellet or supernatant of lysed, centrifuged cells, respectively [32]. Paclitaxel (a microtubule-stabilising agent) and nocodazole (a microtubule-destabilising agent) were used as controls. As expected, tubulin from nocodazole-treated cells was depolymerized and detected almost wholly in the supernatant, whereas tubulin from paclitaxel-treated cells was polymerized and detected solely in the pellet (Figure 8B). Tubulin from cells treated with **1** (10 μM) was found exclusively in the supernatant, indicating complete depolymerization of tubulin (Figure 8B). Similar results were obtained for 5 μM and 20 μM concentrations of **1**. Equal amounts of tubulin were detected in the supernatants and pellets of cells treated with 1 μM of **1**, indicating that this concentration does not have an effect on tubulin polymerization in MCF-7 and Jurkat cells (data not shown).

Finally, a second cellular assay to examine the effects of **1** on the microtubule network of MCF-7 cells was carried out using immunofluorescence and confocal microscopy. Cells were again treated

with either paclitaxel, known microtubule-destabilising agent **2**, or **1**. Vehicle-treated cells displayed organised microtubule structures (Figure 9). Cells treated with the microtubule-stabilising agent paclitaxel exhibited characteristic bundling, whereas cells treated with **2** showed disruption of the microtubule network. Cells treated with a higher concentration of **1** (20 μM) showed a disorganised microtubule structure, consistent with depolymerised tubulin. A lower concentration of 10 μM caused less depolymerisation, with some polymerised microtubules still present (Figure 9). These results provide further evidence that **1** is a direct microtubule-destabilising agent.

Compound **1** is structurally similar to a number of tubulin-depolymerising agents, including **2**, which bind to the colchicine-binding site on tubulin. Potential binding of **1** at the colchicine-binding site was therefore investigated using a whole-cell based assay. N,N'-Ethylene-bis(iodoacetamide) (EBI) is an alkylating agent that cross-links cysteine residues at positions 239 and 354 in the colchicine-binding site of tubulin, forming a β-tubulin-EBI adduct. This adduct is detectable by Western blotting as an immunoreactive band that migrates faster than β-tubulin. Microtubule-destabilising agents that bind at the colchicine-site, such as **2**, prevent the formation of the β-tubulin-EBI adduct [33]. MCF-7 cells were treated with vehicle control, **2** (10 μM) or **1** (40 μM) for 2 h, followed by EBI for an additional 1.5 h (Figure 10). Control samples show the presence of the β-tubulin-EBI adduct at a lower position, indicating that EBI has cross-linked Cys239 and Cys354 on β-tubulin. Adduct formation was inhibited in cells treated with **2**, confirming that **2** binds to the colchicine-binding site, whereas **1** did not inhibit the formation of the β-tubulin-EBI adduct. Similar results were found in HT-29 cells (Figure 10). This indicates that **1** does not bind at the colchicine-site of tubulin. It is also possible, due to the presence of reactive α,β-unsaturated groups, that compound **1** itself could cross-link cysteine residues on

tubulin. It has a similar molecular weight to EBI (317 and 396 respectively) and so an adduct between β-tubulin and **1** would migrate a similar distance to that of a β-tubulin−EBI adduct. Further work is required to determine where, and how, **1** interacts with tubulin.

3. Conclusion

Piperlongumine (piplartine) **1**, a small molecule which has been receiving huge interest of late, has been shown for the first time to target tubulin, by destabilising microtubules in MCF-7 breast cancer cells and Jurkat T-lymphocytes. This effect was confirmed by in vitro tubulin polymerisation, sedimentation and western blotting, and combined immunofluorescence and confocal microscopy. A series of analogues of **1** were synthesised and evaluated for antiproliferative activity, from which compound **13** was identified as having the best toxicity profile when comparing its effects on viability in MCF-7 breast cancer cells and non-tumorigenic MCF-10a breast epithelial cells. It was also shown that combretastatin A-4 (**2**) and colchicine, established tubulin-destabilising agents, may target the stress response to ROS in MCF-7 breast cancer cells. The results of this work are an important contribution to further understanding the intricate biochemical and biological mechanisms of action of **1**.

4. EXPERIMENTAL METHODS

All reagents were commercially available and were used without further purification unless otherwise indicated. Anhydrous dichloromethane was obtained by distillation from calcium hydride immediately prior to use. ^{1}H and ^{13}C NMR spectra were obtained on a Bruker Avance DPX 400 instrument at 20^{o}C, 400.13 MHz for ^{1}H spectra, 100.61 MHz for ^{13}C spectra, in either $CDCl_3$, CD_3COCD_3 or CD_3OD (internal standard: TMS). HRMS for all final compounds were obtained on a Micromass Time of Flight mass spectrometer (TOF) equipped with electrospray

ionization (ES) interface operated in positive ion mode at the High Resolution Mass Spectrometry Laboratory by Mr. Brian Talbot in the School of Pharmacy, Trinity College Dublin. TLC was performed using Merck Silica gel 60 TLC aluminium sheets with fluorescent indicator visualizing with UV light at 254nm. Flash chromatography was carried out using standard silica gel 60 (230-400 mesh) obtained from Merck. All products isolated were homogenous on TLC. The purity of the tested compounds was determined by HPLC and, unless otherwise stated, the purity level was $\geq$95%. Analytical high-performance liquid chromatography (HPLC) was performed using a Waters 2487 Dual Wavelength Absorbance detector, a Waters 1525 binary HPLC pump and a Waters 717plus Autosampler. The column used was a Varian Pursuit XRs C18 reverse phase 150 x 4.6mm chromatography column. Samples were detected using a wavelength of 254 nm. All samples were analyzed using acetonitrile (70%): water (30%) over 10 min and a flow rate of 1 mL/min.

4.1. N-(But-3-en-1-yl)acrylamide (5)(Ref. [15]). Triethylamine (2.95 mL, 21.12 mmol) was added to a stirred solution of but-3-en-1-amine (1 g, 14.08 mmol) in DCM (20 mL) at 0 °C. Acryloylchloride (1.2 equiv., 1.6 mL, 16.90 mmol) was added and the mixture was allowed to stir at room temperature for 3 hr. The reaction mixture was diluted with water, and then extracted into DCM (2 × 10 mL). The solvent was removed *in vacuo* and the crude product was purified by flash column chromatography on silica gel using CH_2Cl_2: methanol (9:1) to give a yellow liquid (56% yield). ^{1}H NMR ($CDCl_3$) δ 2.26 (2 H, q, *J*=6.7 Hz), 3.36 (2 H, q, *J*=6.7 Hz), 4.99 - 5.12 (2 H, m) 5.59 (1 H, dd, *J*=9.7, 1.0 Hz), 5.74 (1 H, ddt, *J*=17.1, 10.4, 6.7, 6.7 Hz), 6.11 (1 H, dd, *J*=17.1, 10.4 Hz), 6.22 (1 H, dd, *J*=16.8, 1.5 Hz), 6.32 (1 H, s[br]); ^{13}C NMR ($CDCl_3$) δ 33.5, 38.5, 117.0, 126.0, 130.9, 135.1, 165.7; HRMS (ESI): *m/z* calcd for $C_7H_{11}NO + H^+$ $(M + H)^+$: 126.0913; found: 126.0911.

4.2. 5,6-Dihydropyridin-2(1*H*)-one (6)(Ref. [15]). Grubbs-II catalyst (42 mg, 5 mol %) was added to a solution of **5** (0.125 g, 1 mmol) in anhydrous DCM (160 mL) and refluxed for 6 hr under inert conditions. The mixture was stirred for an additional 1 hr at room temperature in open air to deactivate the catalyst. The reaction mixture was filtered through celite, concentrated, and the residue was purified by column chromatography on silica gel using hexane/EtOAc (1:1) to give a brown liquid (52% yield). ^{1}H NMR ($CDCl_3$) δ 2.35-2.36 (2H, m), 3.43 (2H, td, J = 7.0, 2.5 Hz), 5.91 (1H, dd, J=10.0, 2.1 Hz), 6.65 (1H, dt, J=10.0, 4.4 Hz); ^{13}C NMR ($CDCl_3$) δ 23.8, 39.7, 124.8, 141.4, 166.3**;** HRMS (ESI): *m/z* calcd for C_5H_7NO + Na $(M + Na)^+$: 120.0425; found: 120.0419.

4.3. Synthesis of compounds 7-13.

General Method I: To a solution of cinnamic acid analogue (0.875 mmol), in freshly distilled THF (5 mL) was added triethylamine (0.10 mL). Pivaloyl chloride (0.69 mmol) was added at -20°C and the reaction mixture was stirred for 45 min. To a solution of **6** (1.05 mmol) in freshly distilled THF (5 mL) was added n-BuLi (1.2 equiv) at -78°C under inert atmosphere conditions and the reaction was stirred for 45 min. Then, anhydride prepared from the above step was added and the reaction mixture was stirred for 1h. The reaction mixture was quenched with saturated NH_4Cl (2 mL), extracted with ethyl acetate (2 × 10 mL), the organic layer was separated and washed with sat. NaCl (2 x 6 mL) and dried over anhydrous Na_2SO_4. The residue was evaporated *in vacuo* to give a crude product which was finally purified by column chromatography on silica gel using hexane/EtOAc (6:4) as eluent to give yellow solid piperlongumine analogue.

4.3.1. 1-Cinnamoyl-5,6-dihydropyridin-2(1*H*)-one (7) was obtained from **6** and cinnamic acid as a colourless oil (72% yield). ^{1}H NMR ($CDCl_3$) δ 2.45 - 2.52 (2 H, m) 4.05 (2 H, t, J=6.43 Hz) 6.05 (1 H, dt, J=9.85, 1.71 Hz) 6.92 - 6.98 (1 H, m) 7.36 - 7.39 (3 H, m) 7.57 - 7.61 (2 H, m) 7.76 (1 H, d, J=15.34 Hz) ; ^{13}C NMR ($CDCl_3$) δ 24.79 (1 C, s) 41.60 (1 C, s) 121.84 (1 C, s) 125.83 (1 C, s) 128.32 (1 C, s) 128.74 (1 C, s) 130.02 (1 C, s) 135.07 (1 C, s) 143.59 (1 C, s) 145.44 (1 C, s) 165.78 (1 C, s) 168.96 (1 C, s); HRMS (ESI): m/z calcd for $C_{14}H_{13}NO_2$ + Na (M + Na): 250.0838; found: 250.0845.

4.3.2. (E)-1-(3-(2-Methoxyphenyl)acryloyl)-5,6-dihydropyridin-2(1*H*)-one (8) was obtained from **6** and 2-methoxycinnamic acid as a yellow oil (68% yield). ^{1}H NMR ($CDCl_3$) δ ppm 2.44 - 2.51 (2 H, m) 3.89 (3 H, s) 4.04 (2 H, t, J=6.53 Hz) 6.05 (1 H, d, J=10.04 Hz) 6.89 - 6.99 (3 H, m) 7.34 (1 H, t, J=7.78 Hz) 7.53 - 7.64 (2 H, m) 8.10 (1 H, d, J=15.56 Hz) ; ^{13}C NMR ($CDCl_3$) δ ppm 24.78 (1 C, s) 41.61 (1 C, s) 55.48 (1 C, s) 111.02 (1 C, s) 120.58 (1 C, s) 122.09 (1 C, s) 124.08 (1 C, s) 125.88 (1 C, s) 128.85 (1 C, s) 131.25 (1 C, s) 138.96 (1 C, s) 145.28 (1 C, s) 158.45 (1 C, s) 165.77 (1 C, s) 169.39 (1 C, s); HRMS (ESI): m/z calcd for $C_{15}H_{15}NO_3$ + Na (M + Na): 280.0944; found: 280.0951.

4.3.3. (E)-1-(3-(3-Methoxyphenyl)acryloyl)-5,6-dihydropyridin-2(1*H*)-one (9) was obtained from **6** and 3-methoxycinnamic acid as a colourless oil (65% yield). ^{1}H NMR ($CDCl_3$) δ ppm 2.61 - 2.71 (2 H, m) 4.00 (3 H, d, J=2.51 Hz) 4.17 - 4.26 (2 H, m) 6.22 (1 H, d, J=9.54 Hz) 7.05 - 7.16 (2 H, m) 7.36 (1 H, d, J=6.53 Hz) 7.41 - 7.50 (1 H, m) 7.66 (1 H, dd, J=16.06, 2.51 Hz) 7.84 - 7.94 (1 H, m); ^{13}C NMR ($CDCl_3$) δ ppm 24.74 (1 C, s) 41.57 (1 C, s) 55.25 (1 C, s) 112.99 (1 C, s) 116.01 (1 C, s) 121.03 (1 C, s) 122.05 (1 C, s) 125.72 (1 C, s) 129.70 (1 C, s) 136.39 (1 C, s) 143.48 (1 C, s) 145.53 (1 C, s) 159.75 (1 C, s) 165.75 (1 C, s) 168.90 (1 C, s); HRMS (ESI): m/z calcd for $C_{15}H_{15}NO_3$ + Na (M + Na): 280.0944; found: 280.0960.

4.3.4. (E)-1-(3-(4-Methoxyphenyl)acryloyl)-5,6-dihydropyridin-2(1*H*)-one (10) was obtained from **6** and 4-methoxycinnamic acid as a white powder (67% yield). ^{1}H NMR ($CDCl_3$) δ 2.47 (2 H, d, J=5.52 Hz) 3.84 (3 H, s) 4.04 (2 H, t, J=6.53 Hz) 6.05 (1 H, d, J=10.04 Hz) 6.87 - 6.97 (3 H, m) 7.42 (1 H, d, J=15.56 Hz) 7.55 (2 H, d, J=8.53 Hz) 7.74 (1 H, d, J=15.56 Hz); ^{13}C NMR ($CDCl_3$) δ 24.80 (1 C, s) 41.61 (1 C, s) 55.34 (1 C, s) 114.19 (1 C, s) 119.37 (1 C, s) 125.92 (1 C, s) 127.83 (1 C, s) 130.03 (1 C, s) 143.63 (1 C, s) 144.41 (1 C, s) 145.31 (1 C, s); HRMS (ESI): m/z calcd for $C_{15}H_{15}NO_3$ + Na (M + Na): 280.0944; found: 280.0951.

4.3.5. (E)-1-(3-(2,4-Dimethoxyphenyl)acryloyl)-5,6-dihydropyridin-2(1*H*)-one (11) was obtained from **6** and 2,4-dimethoxycinnamic acid as a yellow oil (63% yield). ^{1}H NMR ($CDCl_3$) δ 2.42 - 2.49 (2 H, m) 3.87 (4 H, s) 3.84 (3 H, s) 4.03 (2 H, t, J=6.43 Hz) 6.01 - 6.06 (1 H, m) 6.44 (1 H, d, J=2.07 Hz) 6.49 (1 H, dd, J=8.50, 2.28 Hz) 6.88 - 6.95 (1 H, m) 7.46 - 7.57 (2 H, m) 8.05 (1 H, d, J=15.76 Hz); ^{13}C NMR ($CDCl_3$) δ 24.82 (1 C, s) 41.60 (1 C, s) 55.41 (1 C, s) 55.49 (1 C, s) 98.31 (1 C, s) 105.16 (1 C, s) 117.33 (1 C, s) 119.55 (1 C, s) 126.02 (1 C, s) 130.33 (1 C, s) 139.23 (1 C, s) 145.02 (1 C, s) 159.91 (1 C, s) 162.62 (1 C, s) 165.78 (1 C, s) 169.60 (1 C, s); HRMS (ESI): m/z calcd for $C_{16}H_{17}NO_4$ + Na (M + Na): 310.1050; found: 310.1044.

4.3.6. (E)-1-(3-(3,4-Dimethoxyphenyl)acryloyl)-5,6-dihydropyridin-2(1*H*)-one (12) was obtained from **6** and 3,4-dimethoxycinnamic acid as a pale yellow powder (64% yield). **^{1}H NMR** ($CDCl_3$) δ 2.48 (2 H, tdd, J=6.48, 6.48, 4.25, 1.87 Hz) 3.92 (6 H, d, J=2.07 Hz) 4.05 (2 H, t, J=6.63 Hz) 6.05 (1 H, dt, J=9.74, 1.97 Hz) 6.86 (1 H, d, J=8.29 Hz) 6.94 (1 H, dt, J=9.85, 4.20 Hz) 7.11 (1 H, d, J=2.07 Hz) 7.17 (1 H, dd, J=8.50, 1.87 Hz) 7.42 (1 H, d, J=15.34 Hz) 7.73 (1 H, d, J=15.34 Hz); **^{13}C NMR** ($CDCl_3$) δ 24.80 (1 C, s) 41.61 (1 C, s) 55.88 (1 C, s) 55.93 (1 C, s) 109.89 (1 C, s) 110.93 (1 C, s) 119.54 (1 C, s) 122.93 (1 C, s) 125.90 (1 C, s) 128.10 (1 C, s) 143.93 (1 C, s) 145.34 (1 C, s) 149.10 (1 C, s) 150.99 (1 C, s) 165.85 (1 C, s) 169.05 (1 C, s); HRMS (ESI): m/z calcd for $C_{16}H_{17}NO_4$ + Na (M + Na): 310.1050; found: 310.1043.

4.3.7. (E)-1-(3-(2,4,5-Trimethoxyphenyl)acryloyl)-5,6-dihydropyridin-2(1*H*)-one (13) was obtained from **6** and 2,4,5-trimethoxycinnamic acid as a bright yellow powder (61% yield). **^{1}H NMR** ($CDCl_3$) δ 2.47 (2 H, tdd, J=6.43, 6.43, 4.35, 1.87 Hz) 3.88 (6 H, d, J=1.66 Hz) 3.93 (3 H, s) 4.04 (2 H, t, J=6.43 Hz) 6.04 (1 H, dt, J=9.74, 1.76 Hz) 6.50 (1 H, s) 6.92 (1 H, dt, J=9.74, 4.25 Hz) 7.10 (1 H, s) 7.46 (1 H, d, J=15.76 Hz) 8.11 (1 H, d, J=15.76 Hz); **^{13}C NMR** ($CDCl_3$) δ 24.83 (1 C, s) 41.63 (1 C, s) 56.01 (1 C, s) 56.45 (1 C, s) 56.50 (1 C, s) 96.96 (1 C, s) 110.91 (1 C, s) 115.85 (1 C, s) 119.30 (1 C, s) 126.01 (1 C, s) 138.89 (1 C, s) 143.24 (1 C, s) 145.10 (1 C, s) 152.04 (1 C, s) 154.08 (1 C, s) 165.84 (1 C, s) 169.45 (1 C, s); HRMS (ESI): m/z calcd for $C_{17}H_{19}NO_5$ + Na (M + Na): 340.1155; found: 340.1160.

4.4. Crystal Structure Report for Compound 12. A specimen of $C_{16}H_{17}NO_4$, approximate dimensions 0.050 mm x 0.140 mm x 0.300 mm, was used for the X-ray crystallographic analysis. The X-ray intensity data were measured at 100(2)K using an Oxford Cryosystems low temperature device using a MiTeGen micromount. Bruker APEX software was used to correct for Lorentz and polarization effects. A total of 360 frames were collected. The total exposure time was 7.00 hours. The integration of the data using a monoclinic unit cell yielded a total of 20430 reflections to a maximum θ angle of 26.80° (0.79 Å resolution), of which 2947 were independent (average redundancy 6.932, completeness = 99.5%, R_{int} = 6.24%, R_{sig} = 3.74%) and 2189 (74.28%) were greater than $2\sigma(F^2)$.The final cell constants of a = 10.5660(8) Å, b = 15.5439(12) Å, c = 8.4713(6) Å, β = 96.3752(17)°, volume = 1382.70(18) $Å^3$, are based upon the refinement of the XYZ-centroids of reflections above 20 σ(I).Data were corrected for absorption effects using the Multi-Scan method (SADABS). The ratio of minimum to maximum apparent transmission was 0.919. The calculated minimum and maximum transmission coefficients (based on crystal size) are 0.6850 and 0.7454. CCDC deposition number: 1485303.

The structure was solved and refined using the Bruker SHELXTL Software Package, using the space group $P2_1/c$, with Z = 4 for the formula unit, $C_{16}H_{17}NO_4$.The final anisotropic full-matrix least-squares refinement on F^2 with 192 variables converged at R1 = 4.30%, for the observed data and wR2 = 10.20% for all data. The goodness-of-fit was 1.045. The largest peak in the final difference electron density synthesis was 0.184 $e^-/Å^3$ and the largest hole was -0.290 $e^-/Å^3$ with an RMS deviation of 0.058 $e^-/Å^3$. On the basis of the final model, the calculated density was 1.380 g/cm^3 and F (000), 608 e^-.

4.5. Cell culture. MCF-7 cells were obtained from the ECACC and were cultured in Minimum Essential Media with GlutaMAX™-I (Gibco) supplemented with heat-inactivated foetal bovine serum (10%) (Gibco), penicillin/streptomycin 5000 U/mL (1%) (Gibco) and non-essential amino acids (1%) (Sigma). Jurkat cells were cultured in RPMI 1640 with GlutaMAX™-I (Gibco) supplemented with heat-inactivated foetal bovine serum (10%) (Gibco) and penicillin/streptomycin 5000 U/mL (1%) (Gibco). Cells were maintained at 37 °C in 95% air/5% CO_2.

MCF-10a cells were obtained as a kind gift from Dr. Susan McDonnell, UCD School of Chemical and Bioprocess Engineering and were cultured in Dulbecco's Modified Eagle Medium: Nutrient Mixture F-12 (DMEM/F12; Gibco) supplemented with 5% horse serum (Invitrogen), 20 ng/mL epidermal growth factor (Merck Millipore), 0.5 μg/mL hydrocortisone (Sigma), 100 ng/mL cholera toxin (Sigma), 10 μg/mL insulin (Sigma), and penicillin/streptomycin 5000 U/mL (1%)(Gibco).

4.6. Cell viability studies. Cells were seeded in 96-well plates at a density of 2.5×10^4 cells/mL (200 μL/well). After 24 h, cells were treated with a vehicle control [0.1% (v/v) ethanol] or a range

of drug concentrations. Plates were incubated for 48 h at 37 °C in 5% CO_2. AlamarBlue (20 μL) (Invitrogen) was added 5 h prior to the endpoint of the assay. Fluorescence was read using the Spectramax Gemini plate reader with excitation at 544 nm and emission at 590 nm. Blank fluorescence values were obtained from wells containing only media (200 μL) and alamarBlue (20 μL), and were subtracted from the values obtained for the other wells. The percentage cell viability was calculated for each drug concentration from $FI_{test}/FI_{control}$; FI_{test} is the fluorescence intensity of the drug and $FI_{control}$ is the fluorescence intensity of the control. Experiments were performed in sextuplicate on three independent occasions for determination of the mean values reported.

4.7. Cell cycle analysis by propidium iodide staining and flow cytometry. Cells were seeded in T25 flasks at a density of 1×10^5 cells/mL (5×10^5 cells/flask). After 24 hr, cells were treated with a vehicle control [0.1% (v/v) ethanol] or compound **1** (5, 10 or 20 μM). After treatment for the appropriate time, cell media was removed and cells were trypsinised. Cell media, trypsinised cells and PBS washings were combined and centrifuged at 800*g* for 10 min. The supernatant was discarded and cells were resuspended in ice-cold PBS (200 μL). Fixing agent [ice-cold 70% ethanol in PBS (2 mL)] was added slowly while gently vortexing and cell suspensions were stored at – 20 °C for 24 hr. PBS (2 mL) and FBS (5 μL) were added and cell suspensions were centrifuged at 800*g* for 10 min. The supernatant was carefully removed and cells were resuspended in BD FACSflow (400 μL). Ribonuclease A (1 mg/mL; 25 μL) and propidium iodide (1 mg/mL; 75 μL) were added and the mixtures were incubated in the dark at 37 °C for 30 min. Samples were analysed using filter FL-2 on the BD Accuri C6 flow cytometer (BD Biosciences). Data collection was gated to exclude cellular debris and cell aggregates. At least 10,000 cells per sample were analysed. Data was analysed using BD CellQuest™. Experiments were performed on three independent occasions for determination of the mean values reported.

4.8. Tubulin Polymerization. Tubulin polymerisation was carried out using an assay kit supplied by Cytoskeleton [Tubulin polymerization HTS assay using >97% pure porcine tubulin, OD-based (BK004P)], based on the principal that light is scattered by microtubules to an extent that is proportional to the concentration of the microtubule polymer. Compounds that interact with tubulin alter its polymerisation, and this can be detected using a spectrophotometer. The absorbance at 340 nm at 37°C is monitored. The assay was performed as described in version 2.2 of the tubulin polymerisation assay kit manual [31].

4.9. Sedimentation assay and western blotting (tubulin polymerisation). Tubulin depolymerization was quantified by using a modified version of a previously documented method.[32] MCF-7 cells were seeded in 6-well plates (1×10^6 cells/well) and then treated with vehicle [0.1% ethanol (v/v)] or indicated concentrations of compound **1** (1, 10, 20 μM), paclitaxel (1 μM) or nocodazole (1 μM) for 4 hours. Cells were harvested into MT-preserving buffer (0.1 M PIPES (pH 6.9), 2 M glycerol, 5 mM $MgCl_2$, 2 mM EGTA, 0.5% Triton X-100, and protease inhibitors (Roche Diagnostics Ltd, UK) supplemented with 4 μM paclitaxel to maintain stability of assembled microtubules during isolation. The supernatant containing unpolymerised tubulin was clarified by centrifugation (20,000*g* for 45 min) and separated from the pellet containing polymerized tubulin. The pellet was washed once in MT-preserving buffer before being denatured in PARP buffer (300 μL)(62.5 mM Tris-HCl, pH 6.8, 25% glycerol, 2% SDS, 0.01% bromophenol blue, 6M urea). Samples were stored at -80 °C. Before use 1M DTT (20 μL) was added to both the supernatant and pellet samples. 2X Laemmli buffer (180 μL)(62.5 mM Tris-HCl, pH 6.8, 6 M urea, 2% SDS, 10% glycerol, and 0.01% bromphenol blue) was added to the supernatants. All samples were boiled at 100 °C for 3 min and loaded equally (30 μg protein). Proteins were separated on 12% SDS-PAGE gels and transferred onto PVDF membranes (Millipore).

Membranes were blocked in 5% non-dry fat milk/TBST for 1 h, anti-α-tubulin primary antibody (1:2500) (Millipore) for 2 h and anti-mouse HRP-conjugated secondary antibody (1:2500) (Promega) for 1 h at RT. All blots were probed with anti-GAPDH antibody (1:5000) (Millipore) to confirm equal loading. Proteins were detected using chemiluminescent western blot detection (Clarity Western ECL substrate) (Bio Rad) on the ChemiDoc MP System (Bio Rad). Experiments were performed on three independent occasions.

4.10. Evaluation of expression levels of anti-apoptotic proteins Bcl-2 and Mcl-1. MCF-7 cells were seeded at a density of 5×10^5 cells/flask in T25 flasks. After 48 or 72 hr, whole cell lysates were prepared from untreated cells or cells treated with vehicle control [ethanol (0.1% v/v)] or compound **1** (10 μM). Cells were harvested in RIPA buffer supplemented with protease inhibitors (Roche Diagnostics), phosphatase inhibitor cocktail 2 (Sigma-Aldrich) and phosphatase inhibitor cocktail 3 (Sigma-Aldrich). Equal quantities of protein (as determined by a BCA assay) were resolved by SDS-PAGE (12%) followed by transfer to PVDF membranes. Membranes were blocked in 5% non-dry fat milk/TBST for 1 hr. Membranes were incubated in the relevant primary antibodies at 4 °C overnight, washed, incubated in horseradish peroxidase conjugated secondary antibody for 1 hr at rt, and washed again. Enhanced chemiluminescence was used for detection of protein expression. Western blot analysis was performed using antibodies directed against Mcl-1 (1:1000) (Millipore) or Bcl-2 (1:500) (Millipore) followed by incubation with a horseradish peroxidase-conjugated anti-mouse antibody (1:1000) (Promega, Madison, WI, USA). All blots were probed with anti-GAPDH antibody (1:5000) (Millipore) to confirm equal loading. Proteins were detected using chemiluminescent western blot detection (Clarity Western ECL substrate) (Bio Rad) on the ChemiDoc MP System (Bio Rad). Experiments were performed on three independent occasions.

4.11. Immunofluorescence and confocal microscopy. Confocal microscopy was used to study the effects of drug treatment on MCF-7 cytoskeleton. For immunofluorescence, MCF-7 cells were seeded at 1×10^5 cells/mL on eight chamber glass slides (BD Biosciences). Cells were either untreated or treated with vehicle [1 % ethanol (v/v)], paclitaxel (1 μM), compound **2** (100 nM) or compound **1** (10 or 20 μM) for 16 h. Following treatment cells were gently washed in PBS, fixed for 20 min with 4 % paraformaldehyde in PBS and permeabilised in 0.5 % Triton X-100. Following washes in PBS containing 0.1 % Tween (PBST), cells were blocked in 5 % bovine serum albumin diluted in PBST. Cells were then incubated with mouse monoclonal anti-α-tubulin−FITC antibody (clone DM1A) (Sigma) (1:100) for 2 hr at rt. Following washes in PBST, cells were incubated with Alexa Fluor 488 dye (1:450) for 1 hr at rt. Following washes in PBST, the cells were mounted in Ultra Cruz Mounting Media (Santa Cruz Biotechnology, Santa Cruz, CA) containing 4,6-diamino-2-phenolindol dihydrochloride (DAPI). Images were captured by Leica SP8 confocal microscopy with Leica application suite X software. All images in each experiment were collected on the same day using identical parameters. Experiments were performed on three independent occasions.

4.12. Colchicine-binding site assay. MCF-7 cells were seeded at a density of 1×10^6 cells/well in 6-well plates and incubated overnight. Cells were treated with vehicle control [ethanol (0.1 % v/v)], colchicine, compound **2** or compound **1** (all 10 μM) for 2 h. After this time, selected wells were treated with *N,N'*-ethylene-bis(iodoacetamide) (EBI) (Santa Cruz Biotechnology) for 1.5 h. Following treatment, cells were twice washed with ice-cold PBS and lysed by addition of Laemmli buffer. Samples were separated by SDS-PAGE, transferred to polyvinylidene difluoride membranes and probed with β-tubulin antibodies (Sigma-Aldrich).

4.13. Cell viability assay including pre-treatment with N-acetyl cysteine or Trolox. N-Acetyl cysteine (Sigma) was dissolved in sterile water (100 mM). Trolox (Sigma) was dissolved in ethanol (1 mM). Fresh solutions were prepared for each experiment. MCF-7 cells were seeded in 96-well plates at a density of 2.5×10^4 cells/mL. After 23 h, cells were pre-treated with NAC or Trolox (2 µL) for 1 hr. The remainder of the assay was carried out as described for the 'Cell viability assay' (above).

Supplementary material. Effects of compounds 7-13 on the viability of MCF10a human mammary epithelial cells.

Acknowledgements. This work was supported by the Irish Research Council (GOIPD/2013/188; NMO′B). The Trinity Biomedical Sciences Institute is supported by a capital infrastructure investment from Cycle 5 of the Irish Higher Education Authority's Programme for Research in Third Level Institutions (PRTLI). The skilful technical assistance of Dr. Gavin McManus (confocal microscopy) and Barry Moran (flow cytometry) are gratefully acknowledged.

Abbreviations

EBI: N,N'-Ethylene-bis(iodoacetamide)

NAC: N-Acetyl Cysteine

PI: Propidium Iodide

ROS: Reactive Oxygen Species

STAT3: Signal transducer and activator of transcription 3

Trolox: 6-Hydroxy-2,5,7,8-tetramethylchroman-2-carboxylic acid

References

1. *World Cancer Report 2014*, ed. S. BW and W. CP. Vol. 3. 2014, Lyon, France: International Association of Cancer Research.
2. Bezerra, D.P., et al., *Overview of the therapeutic potential of piplartine (piperlongumine).* European Journal of Pharmaceutical Sciences, 2013. **48**(3): p. 453-463.
3. Raj, L., et al., *Selective killing of cancer cells by a small molecule targeting the stress response to ROS.* Nature, 2011. **475**: p. 231–234.
4. Bharadwaj, U., et al., *Drug-repositioning screening identified piperlongumine as a direct STAT3 inhibitor with potent activity against breast cancer.* Oncogene, 2014. **0**.
5. Halasi, M., et al., *ROS inhibitor N-acetyl-L-cysteine antagonizes the activity of proteasome inhibitors.* Biochem. J., 2013. **454**: p. 201-208.
6. Makhov, P., et al., *Piperlongumine promotes autophagy via inhibition of Akt/mTOR signalling and mediates cancer cell death.* Br J Cancer, 2014. **110**(4): p. 899-907.
7. Wang, Y., et al., *Piperlongumine Suppresses Growth and Sensitizes Pancreatic Tumors to Gemcitabine in a Xenograft Mouse Model by Modulating the NF-kappa B Pathway.* Cancer Prevention Research, 2016. **9**(3): p. 234-244.
8. Ducki, S., et al., *Combretastatin-like chalcones as inhibitors of microtubule polymerization. Part 1: Synthesis and biological evaluation of antivascular activity.* Bioorganic & Medicinal Chemistry, 2009. **17**(22): p. 7698-7710.
9. Hatanaka, T., et al., *Novel B-ring modified combretastatin analogues: Syntheses and antineoplastic activity.* Bioorganic & Medicinal Chemistry Letters, 1998. **8**(23): p. 3371-3374.

10. Punganuru, S.R., et al., *Design and synthesis of a C7-aryl piperlongumine derivative with potent antimicrotubule and mutant p53-reactivating properties.* European Journal of Medicinal Chemistry, 2016. **107**: p. 233-244.

11. Adams, D.J., et al., *Synthesis, cellular evaluation, and mechanism of action of piperlongumine analogs.* Proceedings of the National Academy of Sciences, 2012. **109**(38): p. 15115-15120.

12. Cragg, G.M., D.G. Kingston, and D.J. Newman, *Anticancer Agents from Natural Products*. 2005, Florida: CRC press.

13. O'Boyle, N.M., et al., *Synthesis and Evaluation of Azetidinone Analogues of Combretastatin A-4 as Tubulin Targeting Agents.* Journal of Medicinal Chemistry, 2010. **53**(24): p. 8569 - 8584.

14. Sackett, D.L., *Podophyllotoxin, steganacin and combretastatin: Natural products that bind at the colchicine site of tubulin.* Pharmacology & Therapeutics, 1993. **59**(2): p. 163-228.

15. Rao, V.R., et al., *Synthesis and biological evaluation of new piplartine analogues as potent aldose reductase inhibitors (ARIs).* European Journal of Medicinal Chemistry, 2012. **57**: p. 344-361.

16. Boll, P.M., et al., *Synthesis and molecular structure of piplartine (=piperlongumine).* Tetrahedron, 1984. **40**(1): p. 171-175.

17. Bezerra, D.P., et al., *Piplartine induces inhibition of leukemia cell proliferation triggering both apoptosis and necrosis pathways.* Toxicology in Vitro, 2007. **21**(1): p. 1-8.

18. Shrivastava, S., et al., *Piperlongumine, an alkaloid causes inhibition of PI3 K/Akt/mTOR signaling axis to induce caspase-dependent apoptosis in human triple-negative breast cancer cells.* Apoptosis, 2014. **19**(7): p. 1148-1164.

19. Halasi, M., et al., *ROS inhibitor N-acetyl-L-cysteine antagonizes the activity of proteasome inhibitors.* Biochemical Journal, 2013. **454**(2): p. 201–208.

20. Salum, L.B., et al., *Cytotoxic 3,4,5-trimethoxychalcones as mitotic arresters and cell migration inhibitors.* European Journal of Medicinal Chemistry, 2013. **63**(0): p. 501-510.

21. Edwards, M.L., D.M. Stemerick, and P.S. Sunkara, *Chalcones: a new class of antimitotic agents.* Journal of Medicinal Chemistry, 1990. **33**(7): p. 1948-1954.

22. Alexandre, J., et al., *Novel Action of Paclitaxel against Cancer Cells: Bystander Effect Mediated by Reactive Oxygen Species.* Cancer Research, 2007. **67**(8): p. 3512-3517.

23. Chiu, W.-H., et al., *Vinca alkaloids cause aberrant ROS-mediated JNK activation, Mcl-1 downregulation, DNA damage, mitochondrial dysfunction, and apoptosis in lung adenocarcinoma cells.* Biochemical Pharmacology, 2012. **83**(9): p. 1159-1171.

24. Mi, L., et al., *Cancer Preventive Isothiocyanates Induce Selective Degradation of Cellular α- and ß-Tubulins by Proteasomes.* Journal of Biological Chemistry, 2009. **284**(25): p. 17039-17051.

25. Larocque, K., et al., *Novel Analogue of Colchicine Induces Selective Pro-Death Autophagy and Necrosis in Human Cancer Cells.* PLOS One, 2014. **9**(1): p. e87064.

26. Ha-Na, L., et al., *Heme Oxygenase-1 Determines the Differential Response of Breast Cancer and Normal Cells to Piperlongumine.* Mol. Cells, 2015. **38**(4): p. 327-335.

27. Han, S.-S., et al., *Piperlongumine inhibits proliferation and survival of Burkitt lymphoma in vitro.* Leukemia Research, 2013. **37**(2): p. 146-154.

28. Kong, E.H., et al., *Piplartine induces caspase-mediated apoptosis in PC-3 human prostate cancer cells.* Oncology Reports, 2008. **20**(4): p. 785-792.

29. Bezerra, D.P., et al., *Evaluation of the genotoxicity of piplartine, an alkamide of Piper tuberculatum, in yeast and mammalian V79 cells.* Mutation Research/Genetic Toxicology and Environmental Mutagenesis, 2008. **652**(2): p. 164-174.

30. Gong, L.-H., et al., *Piperlongumine Induces Apoptosis and Synergizes with Cisplatin or Paclitaxel in Human Ovarian Cancer Cells.* Oxidative Medicine and Cellular Longevity, 2014. **2014**: p. 10.

31. *Cytoskeleton*. [cited 2015 19th August]; Available from: http://www.cytoskeleton.com/pdf-storage/datasheets/bk004p.pdf.

32. Minotti, A.M., S.B. Barlow, and F. Cabral, *Resistance to Antimitotic Drugs in Chinese Hamster Ovary Cells Correlates with Changes in the Level of Polymerized Tubulin.* Journal of Biological Chemistry, 1991. **266**(6): p. 3987-3994.

33. Fortin, S., et al., *Quick and Simple Detection Technique to Assess the Binding of Antimicrotubule Agents to the Colchicine-Binding Site.* Biological Procedures Online, 2010. **12**(1): p. 113-117.

TABLES

Table 1. Effects of compound 1 and analogues 7-13 on viability of MCF-7 breast cancer cells

Compound	R_1	R_2	R_3	R_4	IC_{50} (μM)
	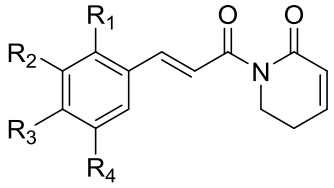				
7	H	H	H	H	3.5 ± 0.8
8	OCH_3	H	H	H	9.6 ± 2.8
9	H	OCH_3	H	H	7.5 ± 1.8
10	H	H	OCH_3	H	8.2 ± 0.1
11	OCH_3	H	OCH_3	H	8.5 ± 1.0
12	H	OCH_3	OCH_3	H	3.7 ± 0.5
13	OCH_3	H	OCH_3	OCH_3	3.4 ± 0.5
PL	H	OCH_3	OCH_3	OCH_3	1.2 ± 0.6

FIGURES

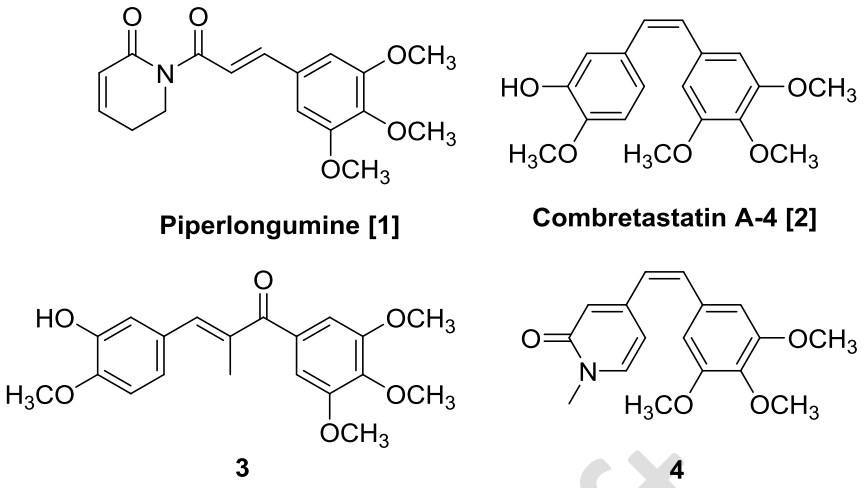

Figure 1. Structures of piperlongumine, combretastatin A-4 and analogues.

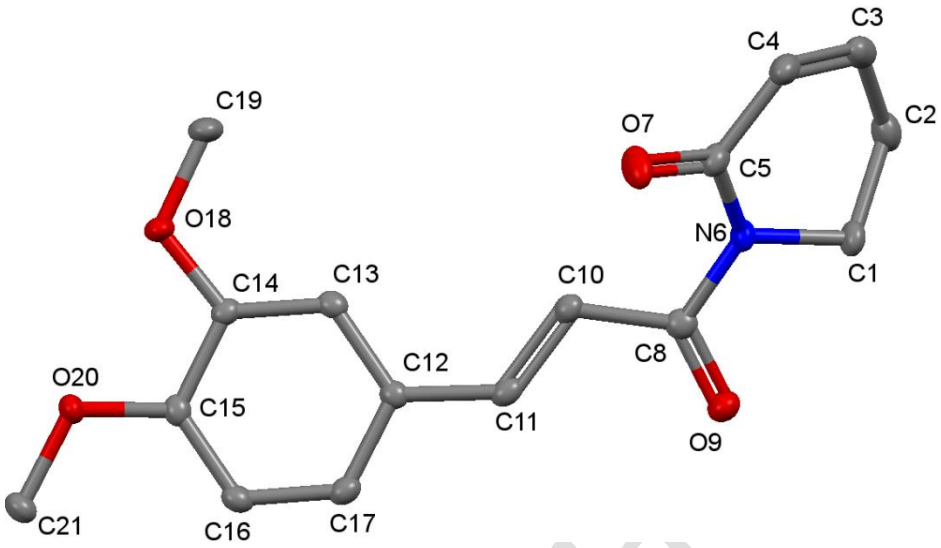

Figure 2. Molecular structure of compound 12 with atomic displacement parameters shown at 50% probability. CCDC deposition number: 1485303.

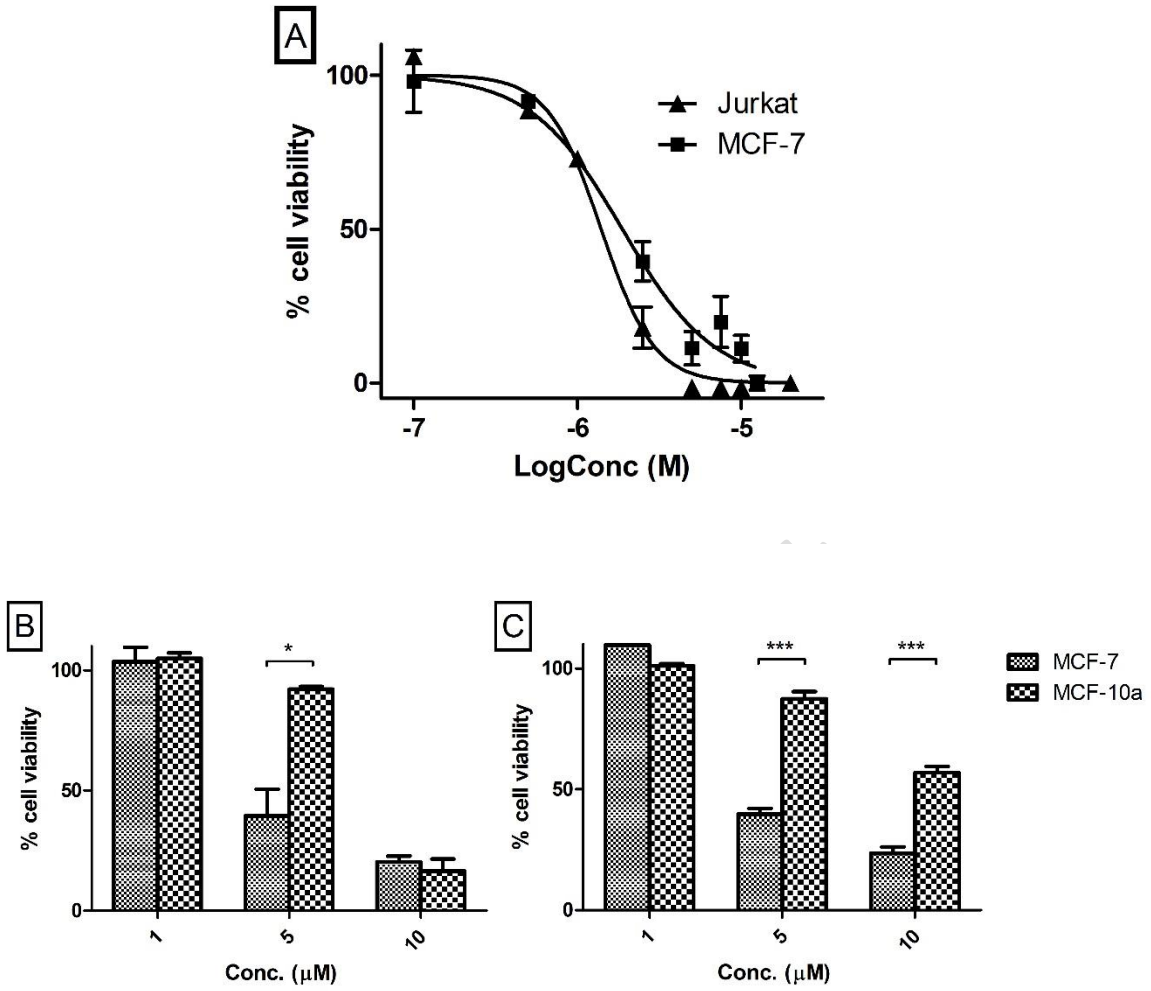

Figure 3A. Compound 1 decreases cell viability of Jurkat and MCF-7 cancer cells. Cells were grown in 96-well plates and treated with compound **1** at 0.1–20 μM for 48 h. Cell viability was expressed as a percentage of vehicle control [ethanol 1% (v/v)] and was measured by alamarBlue assay (average of three independent experiments). **Figure 3B, C. Effects of compounds 7 and 13 on the viability of MCF10a human mammary epithelial cells.** Cells were treated with compound **7** (B) or **13** (C)(1, 5, 10 and 20 μM) for 48 hr. Cell viability was expressed as a percentage of vehicle control [ethanol 1% (v/v)] and was measured by alamarBlue assay (average of three independent experiments). A non-paired two-tailed t-test was used to test for statistical significance (*, $p < 0.05$;***, $p < 0.001$)

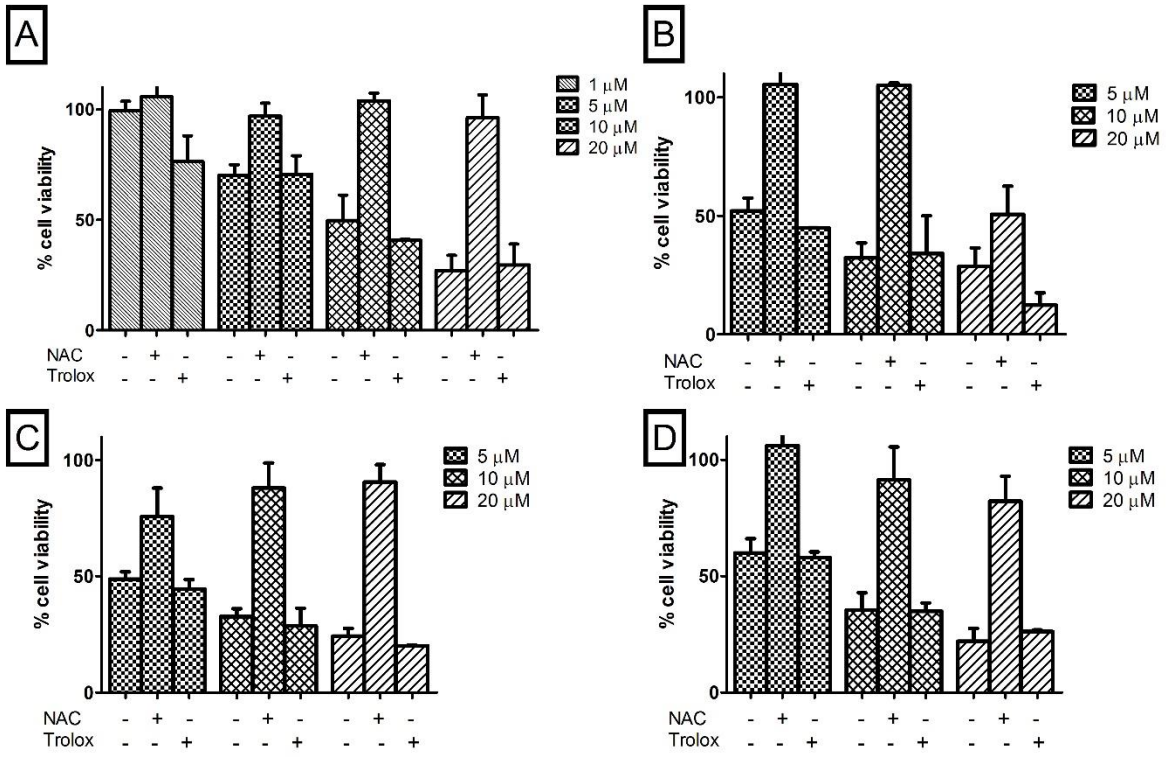

Figure 4. Effect of antioxidant pre-treatment on viability of MCF-7 cells treated with compound 1 or analogues. MCF-7 cells were seeded at a density of 2.5 x 10^4 cells/ ml in 96 well plates and left overnight to adhere. Cells were then pre-treated with NAC (1 mM) or Trolox (100μM) for 1 hr, followed by either compound **1** (A), compound **7** (B), compound **12** (C) or compound **13** (D) at the indicated concentrations for 48 hr. Cell viability was expressed as a percentage of vehicle control [ethanol 1% (v/v)] and was measured by alamarBlue assay (average of three independent experiments).

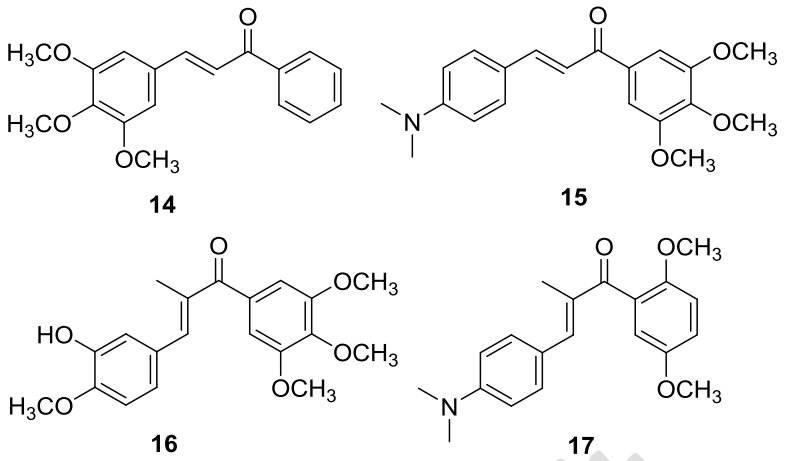

Figure 5. Tubulin-depolymerising chalcones evaluated for effects on ROS

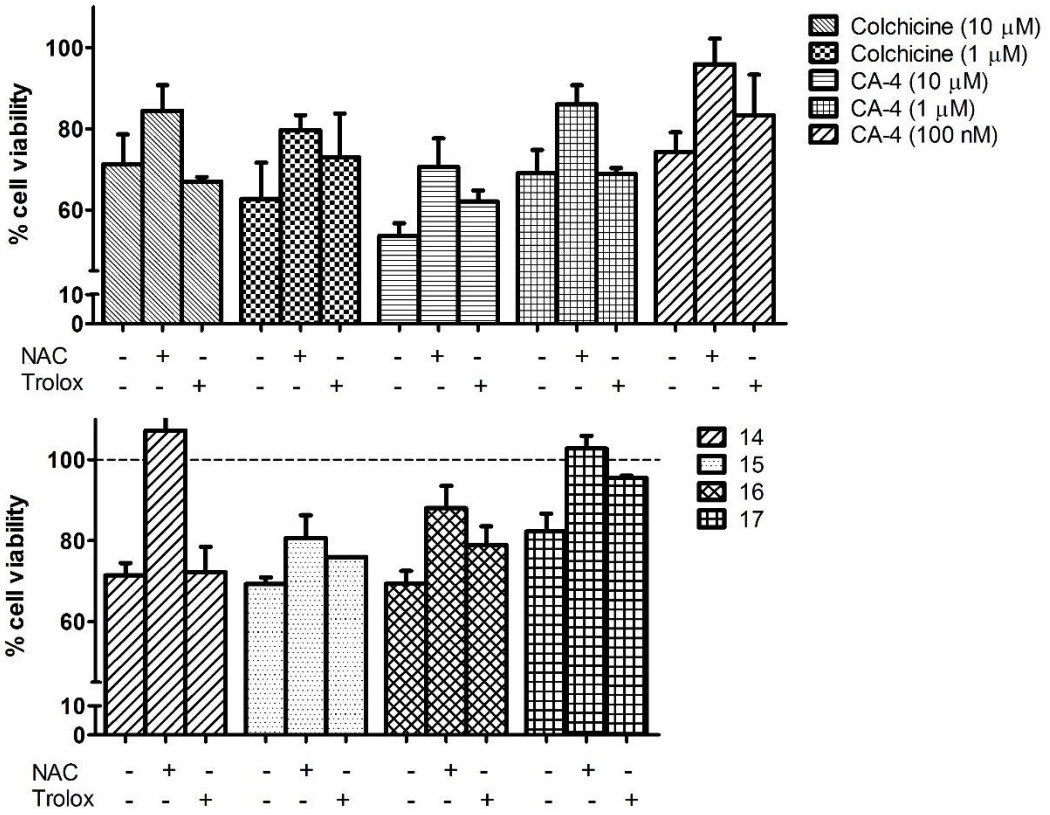

Figure 6. Effect of antioxidant pre-treatment on viability of MCF-7 cells treated with tubulin-depolymerising agents. MCF-7 cells were seeded at a density of 2.5 x 10^4 cells/ ml in 96 well plates and left overnight to adhere. Cells were then pre-treated with NAC (1 mM) or Trolox (100μM) for 1 hr, followed by either colchicine, compound **2**, or compound **14** (10 μM), **15** (10 μM), **16** (10 μM), **17** (10 μM) for 48 hr. Cell viability was expressed as a percentage of vehicle control [ethanol 1% (v/v)] and was measured by alamarBlue assay (average of three independent experiments).

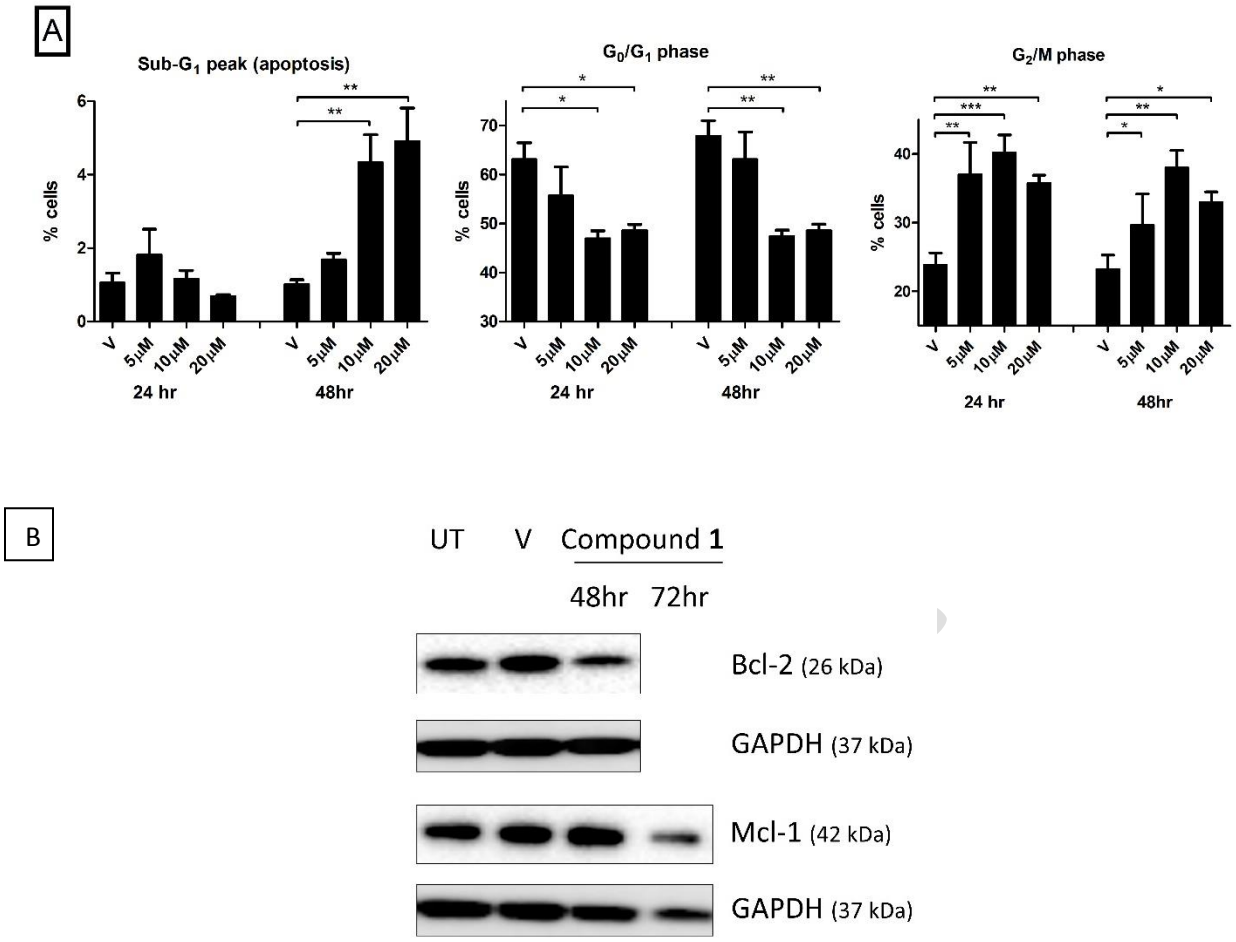

Figure 7.A. Effects of compound 1 on the cell cycle and apoptosis in MCF-7 cells. Cells were treated with either vehicle [V, 0.1% ethanol (v/v)], compound **1** (5, 10 or 20 μM) for 24 or 48 hr. Cells were then fixed, stained with PI, and analyzed by flow cytometry. Cell cycle analysis was performed on histograms of gated counts per DNA area (FL2-A). The number of cells with <2N (sub-G_1), 2N (G_0G_1), and 4N (G_2/M) DNA content was determined with CellQuest software. Values represent the mean ± S.E.M. for three separate experiments. Statistical analysis was performed using one-way ANOVA followed by Dunnett's multiple comparison test; (*, $p < 0.05$;**, $p < 0.01$; ***, $p < 0.001$). **B. Compound 1 downregulates the expression of anti-apoptotic proteins Bcl-2 and Mcl-1.** MCF-7 cells were treated with 10 μM of compound **1**. Untreated (UT) and vehicle (EtOH, 0.1 % v/v) controls were also examined. After the required

time (24 or 48 hr) cells were harvested and separated by SDS PAGE. The membrane was probed with anti-Bcl-2 or anti-Mcl-1 antibodies and transferred to PVDF membrane. The membrane was then re-probed for GAPDH as loading control. Results are representative of three separate experiments.

A.

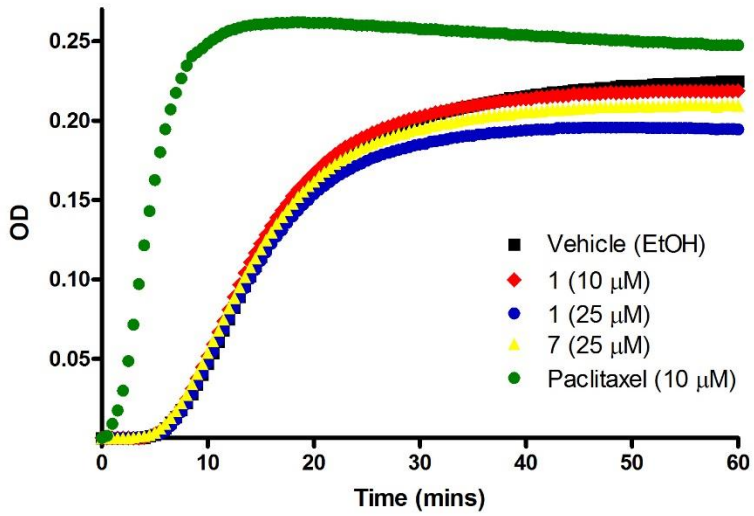

B.

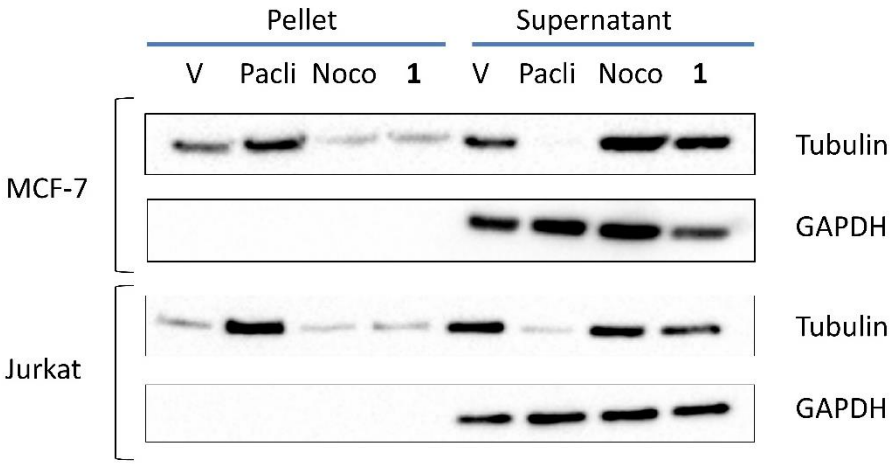

Figure 8. Compound 1 induces depolymerization of tubulin in vitro and in MCF-7 cells. A. Effect of compounds **1** and **7** on in vitro tubulin polymerisation. Purified bovine tubulin and GTP were mixed in a 96-well plate at 37 ^{o}C. Ethanol (1% v/v) was used as a vehicle control. The effect on tubulin assembly was monitored in a Spectramax 340PC spectrophotometer at 340 nm at 30 s intervals for 60 min at 37 ^{o}C. The results represent the mean for three separate experiments

performed in duplicate. B. The effect of compound **1** on microtubule dynamics in MCF-7 breast cancer cells and Jurkat T-lymphocytes was examined by a sedimentation assay and western blotting. Cells were treated with vehicle [0.1% ethanol (v/v)], **1** (10 μM), paclitaxel or nocodazole (1μM) for 4 hr before being lysed in MT preserving buffer. Depolymerized and polymerized fractions were separated by centrifugation and collected as supernatant and pellet fractions respectively. Samples were separated by western blotting and probed with anti-α-tubulin antibody [1:1000] and anti-mouse secondary antibody [1:1000]. GAPDH was used as a loading control [1:1000]. Results are representative of three separate experiments.

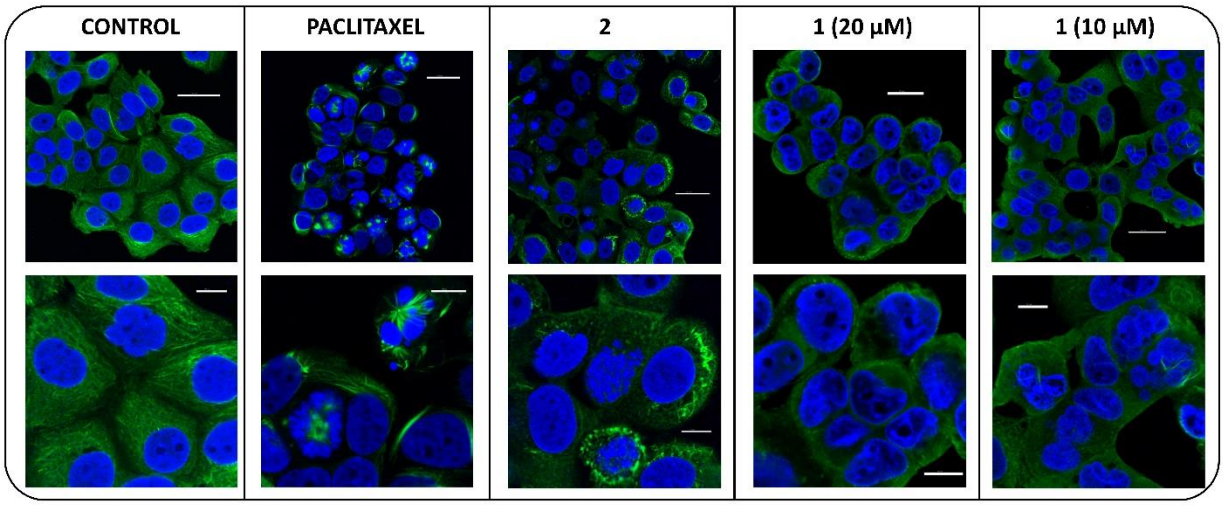

Figure 9. Compound 1 depolymerises the microtubule network of MCF-7 breast cancer cells. Cells were treated with vehicle control [1% ethanol (v/v)], paclitaxel (1 μM), compound **2** (100 nM) or compound **1** (10 or 20 μM) for 16 h. Cells were fixed in 4% paraformaldehyde and stained with mouse monoclonal anti-α-tubulin−FITC antibody (clone DM1A) (green), Alexa Fluor 488 dye and counterstained with DAPI (blue). Images were captured by Leica SP8 confocal microscopy with Leica application suite X software. Representative confocal micrographs of three separate experiments are shown. Scale bar: 30 μM (top images); 10 μM (bottom images).

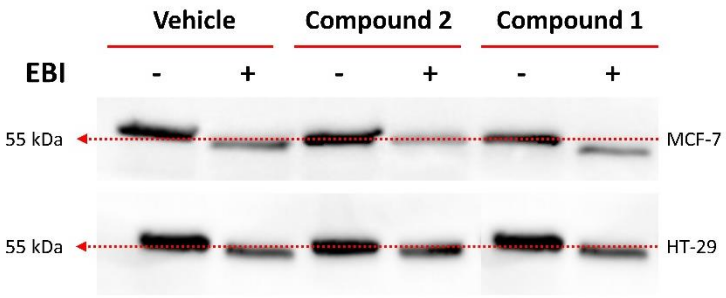

Figure 10. Effects of compound 1 on the inhibition of the bisthioalkylation of Cys239 and Cys354 of β-tubulin by *N,N'*-ethylene-bis(iodoacetamide) (EBI) in MCF-7 and HT-29 cells. MCF-7 and HT-29 cells were treated with vehicle control [ethanol 0.1% (v/v)], **2** (10 μM) or **1** (40 μM) for 2 h; selected samples were then treated with EBI for an additional 1.5 h. Cells were harvested, lysed and analysed using sedimentation and Western blotting for β-tubulin and β-tubulin-EBI adduct. Results are indicative of three separate experiments, performed independently.

SCHEMES

Scheme 1. Synthesis of compound 1 and analogues 7-13[a]

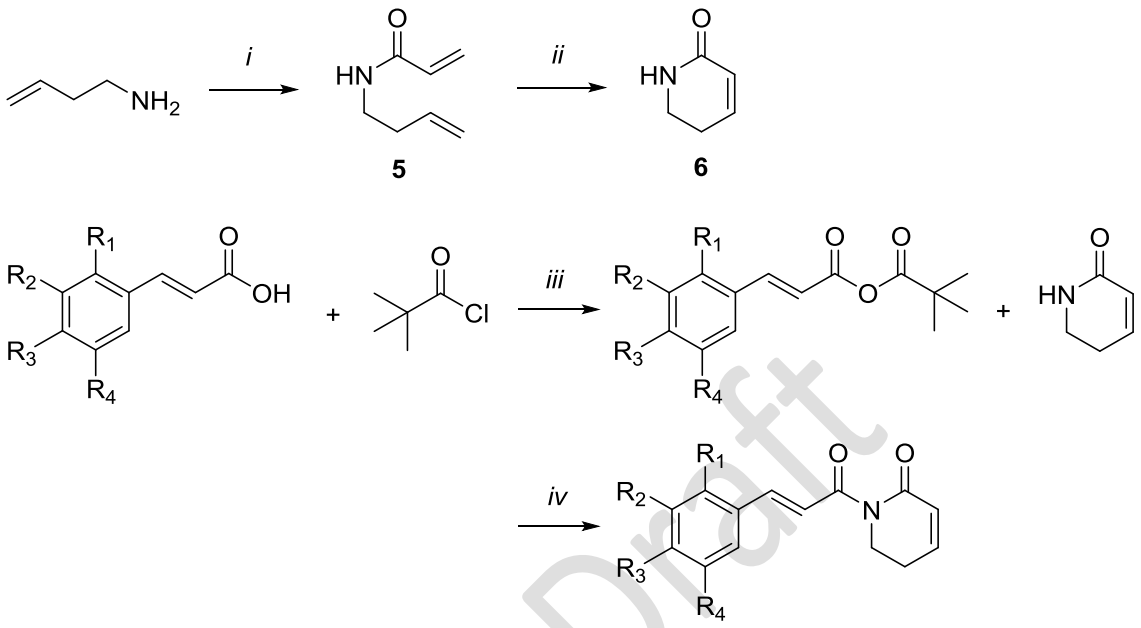

[a]*(i) $CH_2CHCOCl$, NEt_3 , DCM, 0 °C to rt, 3 hr, 56%; (ii) Grubbs catalyst (2nd generation), DCM, reflux, 6 hr, 52%; (iii) NEt_3, THF, -20°C, 45 min; (iv) n-BuLi, THF, -78°C, 45 min; anhydride addition, 1 hr, 61-72%*